Online Eccentricity Monitoring of Seamless Tubes in Cross-Roll Piercing Mill

Weihong Guo[1]
Department of Industrial and Operations Engineering,
The University of Michigan,
Ann Arbor, MI 48109
e-mail: graceguo@umich.edu

Rui Chen
Manufacturing Engineering Program of Integrative Systems and Design Division,
College of Engineering,
The University of Michigan,
Ann Arbor, MI 48109
e-mail: ruichen@umich.edu

Jionghua (Judy) Jin
Fellow ASME
Department of Industrial and Operations Engineering,
The University of Michigan,
Ann Arbor, MI 48109
e-mail: jhjin@umich.edu

Wall-thickness eccentricity is a major dimensional deviation problem in seamless steel tube production. Although eccentricity is mainly caused by abnormal process conditions in the cross-roll piercing mill, most seamless tube plants lack the monitoring at the hot piercing stage but only inspect the quality of finished tubes using ultrasonic testing (UT) at the end of all manufacturing processes. This paper develops an online monitoring technique to detect abnormal conditions in the cross-roll piercing mill. Based on an image-sensing technique, process operation condition can be extracted from the vibration signals. Optimal frequency features that are sensitive to tube wall-thickness variation are then selected through the formulation and solution of a set-covering optimization problem. Hotelling T^2 control charts are constructed using the selected features for online monitoring. The developed monitoring technique enables early detection of eccentricity problems at the hot piercing stage, which can facilitate timely adjustment and defect prevention. The monitoring technique developed in this paper is generic and can be widely applied to the hot piercing process of various products. This paper also provides a general framework for effectively analyzing image-based sensing data and establishing the linkage between product quality information and process information.
[DOI: 10.1115/1.4028440]

Keywords: feature extraction, Hotelling T^2 control charts, online image sensing, seamless tube, cross-roll piercing

1 Introduction

Seamless steel tubes have been widely used in various applications such as boiler tubes, oil drilling, oil pipelines, automobile and aircraft pipelines, etc. The cold-finished seamless tubes possess exceptional strength-to-weight ratios, excellent surface quality, and dimensional accuracy and are available with a wide range of mechanical properties [1]. Producing seamless tubes, however, involves huge complexities and challenges, especially under high pressure and high temperature working environments. Besides mechanical properties, end users of seamless steel tubes also require high-quality tubes with increasingly accurate dimensions.

In a typical seamless tube plant, tube quality is inspected at the end of manufacturing processes through off-line ultrasonic testing (UT) in order to ensure tube quality satisfies customer requirements. Tube quality is affected by almost all processes from hot forming to cold extrusion and finishing. Minor dimensional defects from hot forming may be corrected in cold finishing. Severe wall-thickness eccentricity, however, is a major yet common dimensional defect from hot forming that may not be easily corrected in downstream processes. In seamless tube production, hot forming usually consists of three steps: cross-roll piercing, elongation, and sizing. The cross-roll piercing invented by the Mannesmann brothers toward the end of the 1880s [1,2] is a widely used efficient technique for producing seamless tubes in various size ranges. Figure 1 shows a schematic representation of the cross-roll piercing process. After heating the starting material (round ingots) to rolling temperature in a rotary heating furnace, the hot solid bar is pierced by means of an internal plug and two specially contoured work rolls, which are driven in the same direction of rotation [3]. The round stock is thrust into the mill by the tapered inlet section of the rolls and formed in a spiral motion over the piercing mandrel to produce the hollow shell. More details and recent studies about the cross-roll piercing process can be found in Refs. [2–7]. Wall-thickness eccentricity is mainly caused by abnormal process conditions in cross-roll piercing, such as the degradation of the piercing mandrel, the wear of work rolls and support roll and shoe, abnormal temperature gradient along the piercing billet, roller setting errors, etc.

Although eccentricity problems surface right after the hot piercing process, they can only be identified from UT results, which are available approximately 2 weeks after hot piercing. If the hot piercing process runs abnormally, process engineers may be hardly aware of this problem before analyzing UT results. This leads to delayed detection of abnormal conditions and thus aggravated eccentricity problems in seamless tube production. Therefore, the cross-roll piercing mill needs to be equipped with advanced process monitoring techniques so that abnormal process conditions responsible for wall-thickness eccentricity can be detected at the early stage within the hot piercing mill.

It is very challenging to deploy a reliable monitoring system in the cross-roll piercing mill due to the movement of the pierced billet and the high temperature, often ranging from 800 to 1200 °C. In the past 20 years, online monitoring of tube/shell wall thickness in hot forming steps has become feasible thanks to the development of nondestructive testing and noncontact testing techniques [8,9] including electromagnetic acoustic transducers [10,11], radiation transmission-based gauges, and laser-ultrasonic gauges. The radiation transmission-based measurement system [12] using isotope as the radiation source has been popularly used in large-scale tube mills. Over the last decade, laser-ultrasonic gauge systems [13] have also been developed. However, the applications of the above techniques are limited due to the large dimensions and high cost of the measurement systems.

With the recent rapid advancement of vision-based sensing systems, image inspection techniques have been increasingly used in hot piercing processes in small-scale and medium-scale mills at relatively low cost [14]. With special optical designs, the

[1]Corresponding author.

Contributed by the Manufacturing Engineering Division of ASME for publication in the Journal of Manufacturing Science and Engineering. Manuscript received April 21, 2014; final manuscript received August 22, 2014; published online December 12, 2014. Assoc. Editor: Robert Gao.

advanced image-based sensing technique is capable of capturing the image of an object that is under high temperatures (as hot as 1450 °C) with the same image quality as if the object were at room temperature. As illustrated in Fig. 1, this sensing technique captures subimages of segments of the pierced tube continuously during the process with a high-speed camera. Since the outer dimension of the hot shell is determined by the hot shell object's edges, these subimages can be aligned to show the overall outer dimension of the hot shell after piercing. Therefore, the tubes' dimensional variation resulted from the hot piercing operation is sensitive to vibration patterns of the hot shell object's edges that can be captured by this image-based sensing technique. This image-based sensing technique has been successfully applied in hot rolling processes for online detection of seam defects [15] and repeating surface defects [16], classification of multiple surface defects [17], and vibration monitoring [18]. It has also been employed in continuous casting processes for automatic classification of surface defects [19] and online bleeds detection [20]. This sensing technology, however, has not been fully used for eccentricity monitoring of seamless tubes in hot piercing processes.

This paper aims to develop an online monitoring technique to detect abnormal conditions in the cross-roll piercing mill. Using the image-based sensing technique, rich information about the hot piercing operation conditions can be extracted. With UT results available at the model training stage, the relationship between product quality and process information can be established through feature selection and statistical quality control methods. Hotelling T^2 control charts are then constructed for online process monitoring and detecting eccentricity problems in the cross-roll piercing mill.

The remainder of this paper is organized as follows. Section 2 describes the product quality information obtained from UT results and operation condition information extracted from the vibration signals at the hot piercing stage. Section 3 presents the proposed methodology for online eccentricity monitoring, including quality classification, monitoring feature selection, and control chart development. In Sec. 4, the proposed methodology is demonstrated through case studies. Section 5 discusses the robustness of the proposed monitoring technique in practice and Sec. 6 concludes the paper.

2 Data Description

In most seamless tube plants, ultrasonic thickness testing (UT) is performed as one of the mandatory tests to ensure the finished tubes meet customers' requirements. Figures 2(*a*) and 2(*b*) show the UT results of two tested tubes, which are the wall-thickness measurements along the tubes' longitudinal direction. The upper and lower specification limits are predetermined by the customers' requirements on wall-thickness. If almost all of wall-thickness measurements along the tube are within the specification limits, as shown in Fig. 2(*a*), the finished tube is considered as conforming, i.e., this tube satisfies the customer's requirement. If some segments of wall-thickness measurements are found beyond the specification limits, as shown in Fig. 2(*b*), the tube is considered as nonconforming, i.e., this tube fails to meet customer's requirement. The nonconforming scenario is often interpreted as the occurrence of large variations of wall-thickness at some segments of the tube. This type of tube thickness variations is usually caused by excessive eccentric vibration of the tube during the hot piercing operation.

To quantify tube quality, the original UT measurements need to be preprocessed so that the extent of wall-thickness variation can be quantified. Figure 3(*a*) is an enlarged view of a section of the original UT data from Fig. 2(*b*). It is noticed that the original UT data consist of upper points and lower points, which represent the maximum wall-thickness and the minimum wall-thickness at each cross section along the tube, respectively. As illustrated in Fig. 3, the maximum wall-thickness for cross section j is denoted as $U_u(j), j = 1, 2, \ldots, L$, where L is the number of measured cross

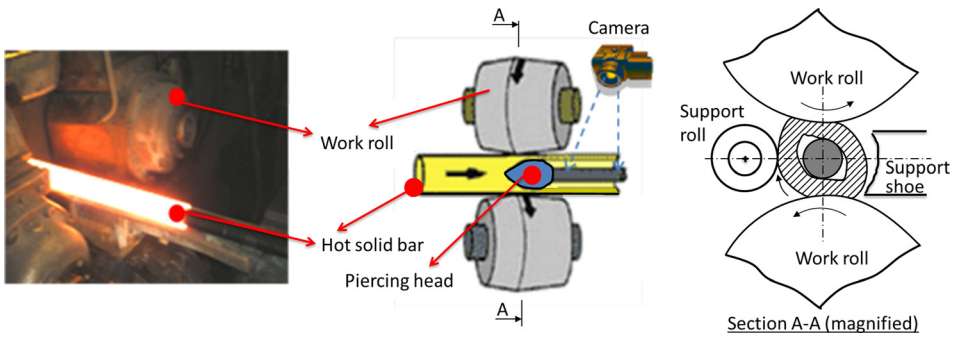

Fig. 1 Seamless tube cross-roll piercing operation and image sensing

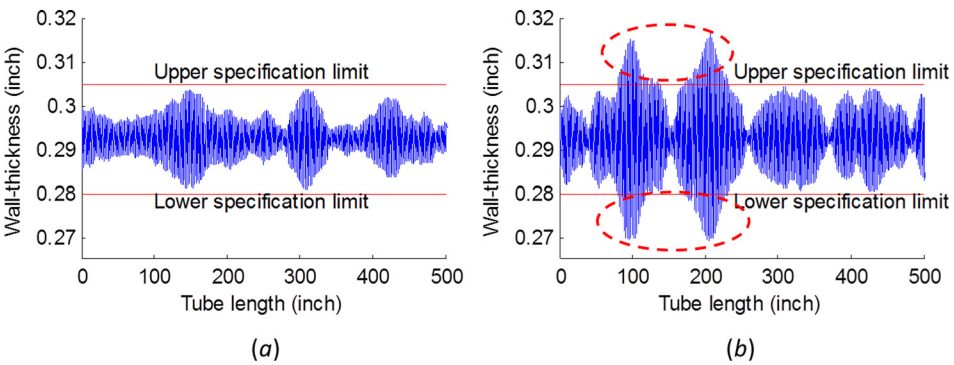

Fig. 2 Examples of UT inspection results: (*a*) a conforming tube and (*b*) a nonconforming tube

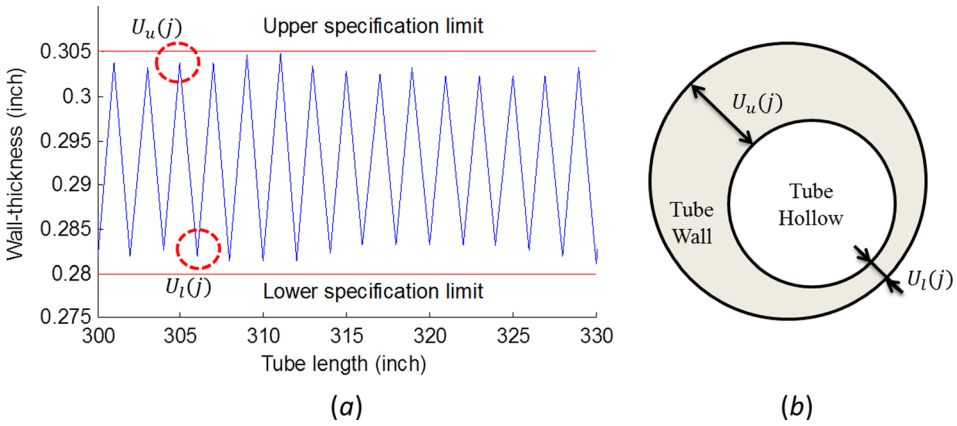

Fig. 3 Wall-thickness variation due to cross section eccentric errors: (*a*) segmental view of thickness variation of Fig. 3(*b*) and (*b*) cross section *j*

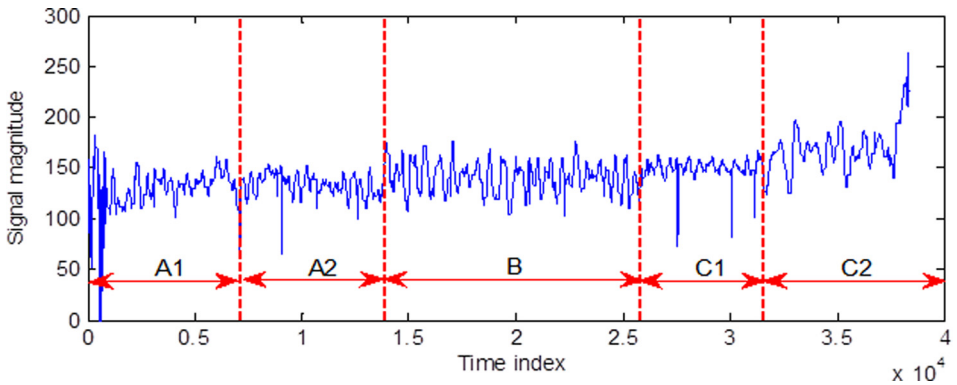

Fig. 4 Vibration signal of a hot pierced tube

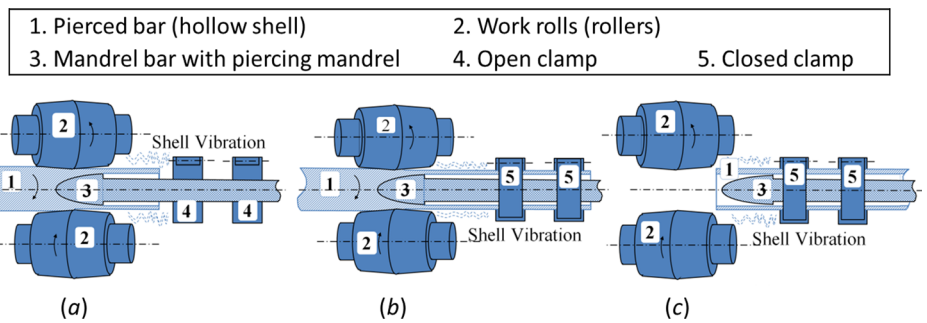

Fig. 5 Three substages of hot piercing: (*a*) billet supported only by rollers, (*b*) billet supported by both rollers and clamps, and (*c*) billet supported only by clamps

sections of the tube; the minimum wall-thickness for cross section j is denoted as $U_l(j), j = 1, 2, \ldots, L$. Hence, the range of wall-thickness variation for cross section j, denoted as $U(j)$, can be calculated as $U(j) = U_u(j) - U_l(j)$. The data series of $\{U(j), j = 1, 2, \ldots, L\}$ represent the range of the wall-thickness variation along the tube length.

Since UT is only performed for final products inspection at the end of all production processes, there is approximately a 2-week delay from hot piercing to available UT results due to the time needed for UT. Therefore, wall-thickness variation range data $\{U(j), j = 1, 2, \ldots, L\}$ cannot be used for online monitoring of the hot piercing operation. For the purpose of online process monitoring, image-based sensing technique is used to capture vibration signals of the pierced tube/shell during the hot piercing operation. As shown in Fig. 4, the vibration signal of a hot pierced tube consists of the signals from five substages of hot piercing operation, denoted as substages A1, A2, B, C1, and C2. Figure 5 illustrates the relative positions of the pierced billet, work rolls, and clamps for each substage. It is noticed that only at substage B the pierced bar is supported by both the work rolls and clamps, while at substages A1, A2, C1, and C2 the pierced bar is supported by either only the work rolls or only the clamps. Therefore, the dynamic characteristics of the tube's vibration are dramatically changed in substages A1, A2, C1, and C2. When the pierced bar is fully supported at substage B, the captured vibration signal is more stationary and thus can be used for monitoring feature extraction.

After the hot piercing operation, for the ease of material handling, a load of 5–50 tubes will be sent together to downstream stations, where multiple cold extrusion operations are performed

to further shape the tube's inner and outer diameters close to the designed values. As a result, all tubes within a load are mixed after the hot piercing station. As we discussed above, each tube vibration signal is captured online at the hot piercing station, and UT is performed at the final station. Consequently, the collected UT data and vibration signals are hardly tube-to-tube mapped, but only load-to-load mapped instead. For the purpose of studying the relationship between the tube's thickness variation and vibration signals, four batches of tube-to-tube mapped data were purposely collected by adding special coding to each individual tube. These tube-to-tube mapped data will be used for model training and validation.

3 Methodology Development

3.1 Overview of the Proposed Methodology. A general framework of the proposed methodology is shown in Fig. 6. The proposed monitoring method aims to quickly detect abnormal conditions of the hot piercing operation, which may potentially lead to a large variation of tube wall-thickness no matter what individual customer's quality requirement is. For this purpose, the first step in the methodology development is to classify tube quality into two groups based on wall-thickness variations $U(j), (j = 1, 2, \ldots, L)$, in which the classified low-quality tubes reflect relatively high variability of wall-thickness while the classified high-quality tubes reflect relatively low wall-thickness variability. At the second step, monitoring features in the frequency domain are extracted from the vibration signals so that these features can be efficiently used to detect the classified low-quality tubes but generate small false alarms for the classified high-quality tubes. The third step is to develop a control chart for online monitoring using the selected features. The detail of each step will be elaborated in Secs. 3.2, 3.3, and 3.4.

3.2 Tube Quality Classification. It is critical to adequately classify tubes into low-quality and high-quality tubes so that the classified low-quality tubes reflect the group of tubes having a relatively higher wall-thickness variation than that of high-quality tubes. Figure 7 shows the major steps for classifying tube quality using a clustering method. Specifically, for a batch of N tubes, $U_k(j)$ is the wall-thickness variation at cross section j $(j = 1, 2, \ldots, L_k)$ of tube $k(k = 1, 2, \ldots, N)$, and the calculation of $U_k(j)$ is discussed in Sec. 2. When tubes have different lengths, however, it is inappropriate to directly compare tube quality using $\{U_k(j), j = 1, 2, \ldots, L_k\}$. Hence, a quality index Q_k is defined based on $\{U_k(j), j = 1, 2, \ldots, L_k\}$ so that it can be used to describe the extent of the wall-thickness variation of tube k. Based on the defined Q_k, a systematic clustering method is then utilized to classify these N tubes into high-quality tubes (Ω_0) and low-quality tubes (Ω_1).

Figure 8 shows four typical patterns of wall-thickness variations: Figure 8(*a*) shows a typical high-quality tube with small wall-thickness variation along the entire tube; Fig. 8(*b*) shows a typical low-quality tube with large wall-thickness variation along the entire tube. Figure 8(*c*) shows a scenario when large wall-thickness variation is spotted only at one cross section of the tube (or in a very small segment of the tube). Considering this point as an outlier since this scenario is highly unlikely to be associated with tube eccentricity, we still regard Fig. 8(*c*) as a high-quality tube. Figure 8(*d*) shows a scenario when large wall-thickness variation is found in about 6% of the tube length. Considering 6% as quite a large proportion and that this scenario may be associated with tube eccentricity, we regard Fig. 8(*d*) as a low-quality tube. Hence, the proposed quality index Q_k should be able to give large values for scenarios (b) and (d) but small values for scenarios (a) and (c). It can be easily seen that the conventional statistics, such as standard deviation $s_k = \sqrt{(1/L_k)\sum_{j=1}^{L_k}(U_k(j) - \bar{U}_k)^2}$ or range $R_k = \max(U_k(j)) - \min(U_k(j))$, cannot be adequately used since R_k is also large for scenario (c) besides (b) and (d), thus leading to a misjudgment of poor quality under scenario (c); while s_k is relatively small for scenario (d), thus leading to a misjudgment of high quality under scenario (d). To overcome the drawbacks of R_k and s_k, we propose the quality index to be $Q_k = U_{p,k}$, where $U_{p,k}$ satisfies

$$\Pr\left(U_k(j) < U_{p,k}, j = 1, 2, \ldots, L_k\right) = 1 - p \tag{1}$$

Hence, $U_{p,k}$ is the $(1-p)$th percentile of $\{U_k(j), j = 1, 2, \ldots, L_k\}$. $U_{p,k}$ represents a percentile statistic to describe the extent of wall-thickness variation in tube k, which is sensitive to out of control conditions leading to large wall-thickness variation found in more than p proportion of the tube length. In other words, if less than p proportion of the tube shows large wall-thickness variation, it would be hardly related to out of control conditions, but instead those points are considered as outliers, thus $U_{p,k}$ still yields a small value. The value of p is determined by the process design requirement. For example, a tube is considered as high quality if large wall-thickness variation is found in less than 5% of the tube length, thus $p = 5\%$. Equivalently, $U_{5\%,k}$ gives a threshold value that 95% of the wall-thickness variation data $\{U_k(j), j = 1, 2, \ldots, L_k\}$ are below $U_{5\%,k}$. A classified low-quality tube has a larger value of $U_{5\%,k}$ than the high-quality tubes, indicating that the low-quality tube has larger wall-thickness variation.

Based on $U_{p,k}$, we now classify tubes into low-quality and high-quality. Figure 9(*a*) shows $U_{5\%,k}$ of a batch of $N = 15$ tubes. A

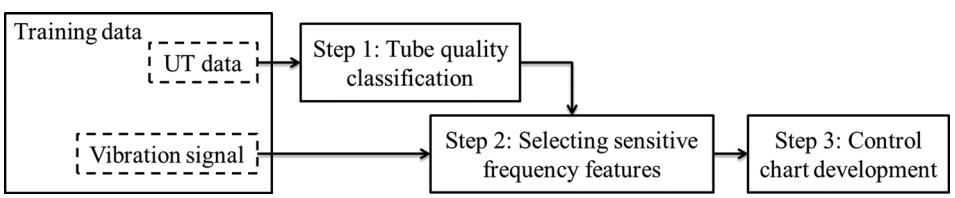

Fig. 6 Flowchart of the proposed methodology

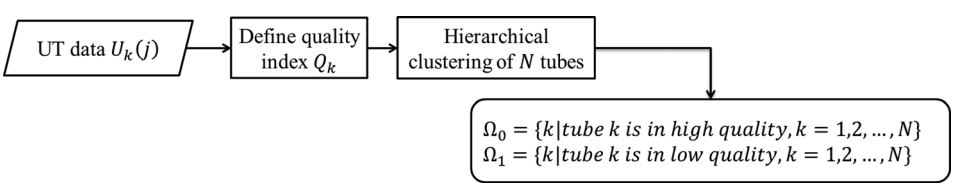

Fig. 7 Flowchart of tube quality classification

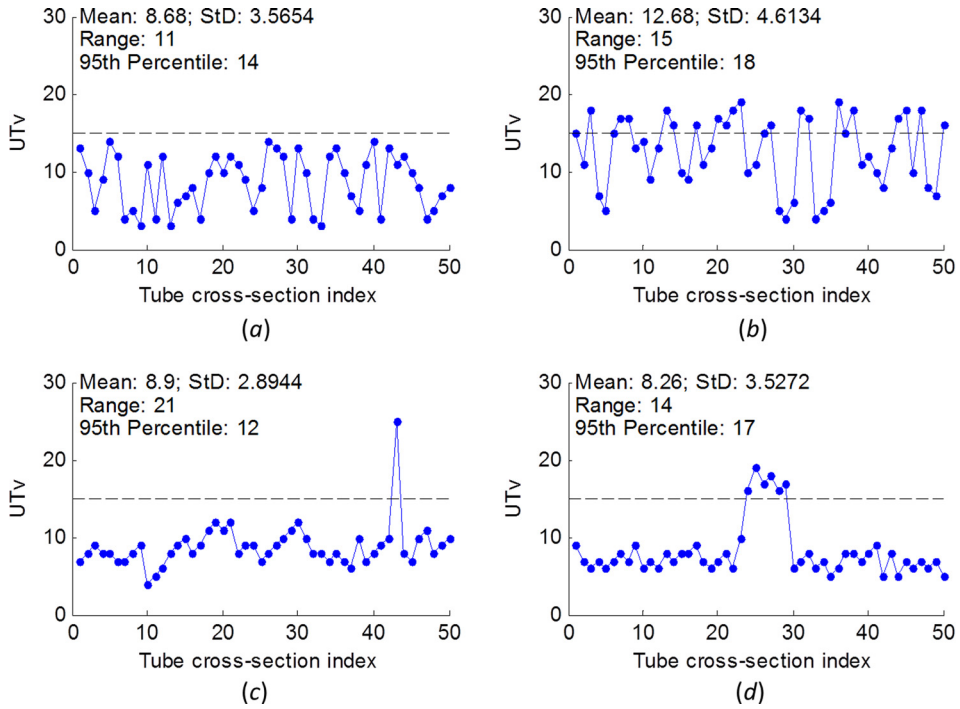

Fig. 8 Patterns of wall-thickness variations: (*a*) a high-quality tube with small wall-thickness variations over the tube, (*b*) a low-quality tube with large wall-thickness variations over the tube, (*c*) a high-quality tube with large wall-thickness variations at only one cross section of the tube, and (*d*) a low-quality tube with large wall-thickness variations over 6% of the tube length

systematic clustering approach is needed instead of using a subjective visual judgment in order to give a consistent benchmark for classifying high-quality and low-quality tubes for different batches. Hierarchical clustering [21] is utilized here for its advantages in unsupervised clustering and good interpretability. After classification, denote the high-quality tubes and low-quality tubes within the batch are $\Omega_0 = \{k|\text{tube } k \text{ is in high quality}, k = 1, 2, \ldots, N\}$ and $\Omega_1 = \{k|\text{tube } k \text{ is in low quality}, k = 1, 2, \ldots, N\}$, respectively.

Figure 9(*b*) shows the hierarchical clustering result of Fig. 9(*a*) data using the Ward's minimum variance method and Euclidean distance between observations. As shown in Fig. 9(*b*), tube#5, 9, 10, 11, 13, and 15 are clustered as low-quality tubes, i.e., $\Omega_1 = \{5, 9, 10, 11, 13, 15\}$, while the rest of tubes in this batch are considered as in high quality, i.e., $\Omega_0 = \{1, 2, 3, 4, 6, 7, 8, 12, 14\}$. It can be seen from Fig. 9(*a*) that this classification gives a cutoff value around 0.032–0.033, which is about 10% of the designed tube wall thickness.

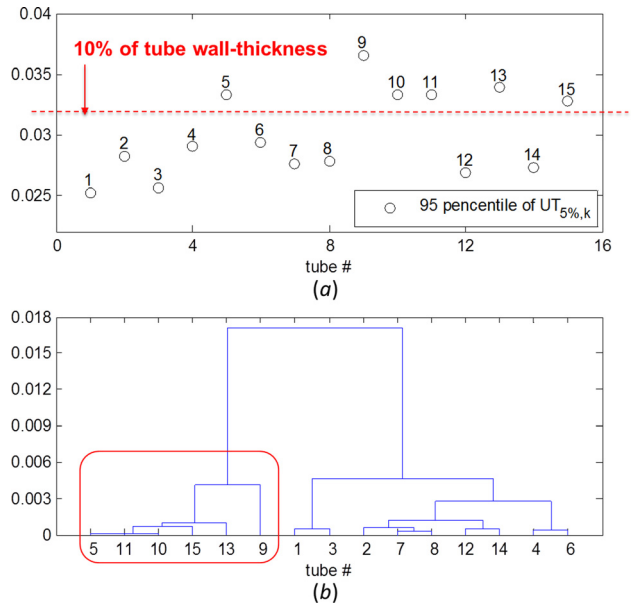

Fig. 9 Hierarchical clustering of a batch of $N = 15$ tubes: (*a*) $U_{5\%,k}$ values and (*b*) dendrogram

3.3 Monitoring Feature Selection. Since large wall-thickness variations are critically affected by abnormal rotating vibration in the hot piercing process, vibration signals are analyzed in the frequency domain. Fast Fourier transform (FFT) [22] is applied on substage B of the vibration signal in order to extract sensitive frequency components as monitoring features. An example of the vibration signal in the frequency domain is shown in Fig. 10. The high magnitudes in features around f_{30} (subscript denotes the feature index) are mainly contributed by the dominant frequency from the rotation of work rolls, but mixing with the rotating movements of the support roll, support shoe, piercing mandrel, and other noises. High magnitudes at harmonic frequencies can also be spotted in Fig. 10.

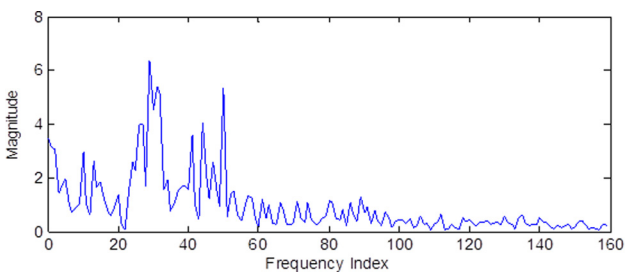

Fig. 10 Vibration signal of substage B shown in frequency domain

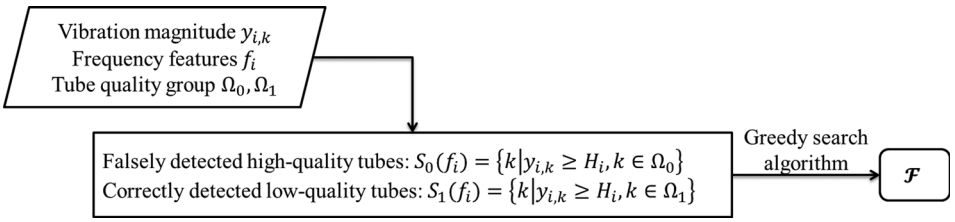

Fig. 11 Flowchart of monitoring feature selection

Based on sampling frequency $\Delta f = 0.3151$ Hz, the frequency features are denoted as f_i (Hz), $f_i = 0.3151 \cdot i, \quad i = 1, 2, \ldots, 160$, where i is the frequency index shown in Fig. 10. A total of 160 frequency features in the range of 0–50 Hz are under consideration. Denote $y_{i,k}$ as the tube k's vibration magnitude at f_i. Obviously, not all frequency features are associated with the thickness variability. In order to detect an abnormal operation of the hot piercing process based on vibration signals, the good monitoring features that can be effectively used to separate Ω_1 from Ω_0 should be selected. One simple approach in feature selection is exhaustive search, which selects the global optimal subset by evaluating all possible subsets at the cost of enormous computation. In this step, we present a greedy search algorithm based on the formulation of a set-covering problem. Figure 11 illustrates the feature selection method in this part, which is described in detail as follows.

For each frequency feature under consideration, $f_i (i = 1, 2, \ldots, 160)$, its vibration magnitude $y_{i,k}$ is compared with a threshold $H_i = \mu_i + K \cdot \sigma_i$, where μ_i is estimated by the sample mean of $y_{i,k \in \Omega_0}$, σ_i is estimated by $(\overline{\text{MR}}/1.128)$ and $\overline{\text{MR}}$ is the arithmetic mean of the moving ranges of $y_{i,k \in \Omega_0}$ values, and K is a constant value setting the width of the allowed dispersion (e.g., $K = 3$). If tube k has $y_{i,k} \geq H_i$, feature f_i will detect tube k as a low-quality tube. Within a batch of N tubes, the monitoring capability of feature f_i is described by two sets

$$\begin{aligned} S_0(f_i) &= \{k | y_{i,k} \geq H_i, k \in \Omega_0\} \\ S_1(f_i) &= \{k | y_{i,k} \geq H_i, k \in \Omega_1\} \end{aligned} \tag{2}$$

$S_0(f_i)$ is a subset of high-quality tubes that are falsely detected by feature f_i as in low quality, while $S_1(f_i)$ is a subset of low-quality tubes that are correctly detected by feature f_i. In the training dataset, f_i and $S_0(f_i)$ are one-to-one mapped, and f_i and $S_1(f_i)$ are also one-to-one mapped. S_0 and S_1 can be considered as a projection from f_i to the set of falsely detected high-quality tubes and the set of correctly detected low-quality tubes, respectively.

Define $\mathcal{F}$ to be the optimal feature set for process monitoring. $\mathcal{F}$ should be able to detect all low-quality tubes in Ω_1, i.e., $\bigcup_{i:f_i \in \mathcal{F}} S_1(f_i) = \Omega_1$. In the meantime, the false alarm number should be kept small while $\mathcal{F}$ should also be concise. In other words, we need to minimize $\left|\bigcup_{i:f_i \in \mathcal{F}} S_0(f_i)\right| + \lambda \sum_{i:f_i \in \mathcal{F}} w(f_i)$, where $\left|\bigcup_{i:f_i \in \mathcal{F}} S_0(f_i)\right|$ is the number of false alarms, λ is a weighting parameter, $\forall i, w(f_i) = 1$, and $\sum_{i:f_i \in \mathcal{F}} w(f_i)$ is the number of features selected.

In a general set-covering problem [23], the input is a finite set $\mathcal{X}$ and a family of subsets of $\mathcal{X}$; and the goal is to find a subset $\mathcal{L}$ that minimizes the objective function while its members cover all of $\mathcal{X}$: $\mathcal{X} = \bigcup_{\mathcal{C} \in \mathcal{L}} \mathcal{C}$. In our monitoring feature selection problem, the constraint on correct detection, $\bigcup_{i:f_i \in \mathcal{F}} S_1(f_i) = \Omega_1$, indicates that the members of the selected subset $S_1(f_i)$ for $i : f_i \in \mathcal{F}$ cover all of Ω_1. Since f_i and $S_1(f_i)$ are one-to-one mapped, the selection of a subset $S_1(f_i)$ is equivalent to the selection of the feature f_i. Hence, the problem of monitoring feature selection can be translated into a set-covering problem defined as finding the set of features, $\mathcal{F}$, in order to

$$\min_{\mathcal{F}} \left| \bigcup_{i:f_i \in \mathcal{F}} S_0(f_i) \right| + \lambda \sum_{i:f_i \in \mathcal{F}} w(f_i)$$

subject to

$$\bigcup_{i:f_i \in \mathcal{F}} S_1(f_i) = \Omega_1 \tag{3}$$

Constraint (3) guarantees that all low-quality tubes are detected by the features in $\mathcal{F}$.

The set-covering problem is a classic optimization problem in computer science and complexity theory for resource selection [23,24]. Although it is an NP-hard problem, there exist several approximation algorithms. Now we give the solution to monitoring feature selection based on a greedy algorithm for the general set-covering problem. Figure 12 illustrates the steps based on the $H(\max_{i=1,2,\ldots,160} |S_1(f_i)|)$—approximation greedy algorithm, where A\B denotes the complement of set B with respect to set A. While the greedy algorithm does not guarantee to find the optimal solution, it guarantees to find a feasible solution that is bounded by a factor $H(\max_{i=1,2,\ldots,160}|S_1(f_i)|)$, where $H(d) = \sum_{i=1}^{d} 1/i$ is the d th harmonic number. By applying the steps in Fig. 12, a feasible solution, $\mathcal{F}$, can be found, which leads to the output of the objective function to be $\left|\bigcup_{i:f_i \in \mathcal{F}} S_0(f_i)\right| + \lambda \sum_{i:f_i \in \mathcal{F}} w(f_i)$. This output is guaranteed to be no greater than $H(\max_{i=1,2,\ldots,160}|S_1(f_i)|)$ times of the optimum.

3.4 Control Chart Development. Figure 13 illustrates the control chart development step in methodology development. A group of control charts is constructed using the selected monitoring features. The phase I performance of control chart is then evaluated with the classified high-quality and low-quality tubes. If the performance satisfies design requirements, the developed model will be used for online process monitoring. Otherwise, the model will be revised in order to achieve a better performance.

The Hotelling T^2 control chart [25] is developed in this section due to its advantages in dealing with multivariate and correlated features. Denote F^* to be the feature set selected in Sec. 3.3, which provides a set of features that is capable of detecting the classified low-quality tubes while maintaining a small false alarm number for the classified high-quality tubes. Though Hotelling T^2 control chart performs well for multivariate process monitoring and control, the control charts work well when the number of process variables is not too large. Therefore, we construct a Hotelling T^2 control chart for each feature interval, $F_r (r = 1, 2, \ldots, R)$.

$V_1 \leftarrow \Omega_1$
$V_0 \leftarrow \Omega_0$
$\mathcal{F} \leftarrow \emptyset$
While $V_1 \neq \emptyset$, do:
Select an f_i that minimizes $\frac{|V_0 \cap (S_0(f_i))| + \lambda}{|(S_1(f_i)) \cap V_1|}$
$V_1 \leftarrow V_1 \backslash \left((S_1(f_i)) \cap V_1\right)$
$V_0 \leftarrow V_0 \backslash \left((S_0(f_i)) \cap V_0\right)$
$\mathcal{F} \leftarrow \mathcal{F} \cup \{f_i\}$

Fig. 12 A greedy algorithm for monitoring feature selection

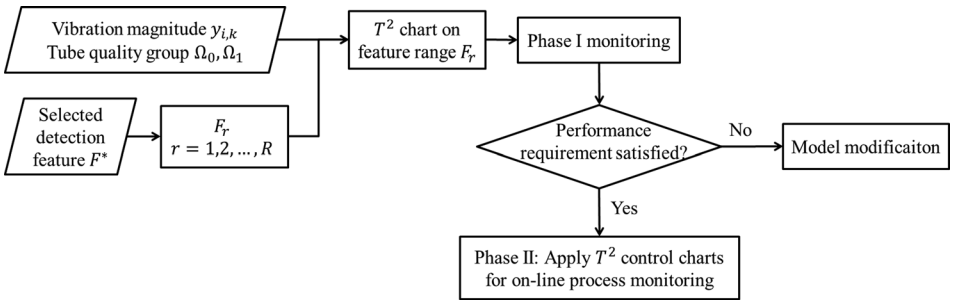

Fig. 13 Procedures for Hotelling T^2 control chart development

Since the frequency features $f_i, i = 1, 2, \ldots, 160$ are extracted from FFT, monitoring features should be a frequency interval containing a number of consecutive f_i's instead of individual features given in F^*. For example, if $F^* = \{42, 44, 46, 47, 87, 90, 92\}$, then we should determine $R = 2$ intervals of frequency features for Hotelling T^2 control chart: one control chart for $F_1 = \{42, \ldots, 47\}$, which covers features 42, 44, 46, and 47; another control chart for $F_2 = \{87 \ldots 92\}$, which covers features 87, 90, and 92. Each feature interval contains six consecutive features covering about 2 Hz of frequencies.

For each feature interval F_r, let $\boldsymbol{x}_{r,k}$ denote the values at features in F_r given by tube k. Let $\bar{\boldsymbol{x}}_r$ and $\boldsymbol{S}_r$ denote the sample mean vector and sample covariance matrix calculated from the high-quality tubes Ω_0 within the batch. The Hotelling T^2 statistic for tube k at feature interval F_r is given as

$$T^2_{r,k} = (\boldsymbol{x}_{r,k} - \bar{\boldsymbol{x}}_r)' \boldsymbol{S}_r^{-1} (\boldsymbol{x}_{r,k} - \bar{\boldsymbol{x}}_r) \tag{4}$$

Within a batch of N_0 high-quality tubes, $|\Omega_0| = N_0$, denote the number of features in F_r as p_r. The phases I and II control limits of Hotelling T^2 control chart at feature interval F_r can be determined by

$$\text{Phase I control limit: } \text{UCL}_r = \frac{(N_0 - 1)^2}{N_0} B_{1-\alpha, \frac{p_r}{2}, \frac{N_0 - p_r - 1}{2}} \tag{5}$$

$$\text{Phase II control limit: } \text{UCL}_r = \frac{p_r (N_0 + 1)(N_0 - 1)}{N_0 (N_0 - p_r)} F_{1-\alpha, p_r, N_0 - p_r} \tag{6}$$

where $B_{(1-\alpha)}$ is the percent point function of the beta distribution and α is the significance level (typically set to 0.05 or 0.01). Lower control limits are not needed since there is no boundary at the lower side. Note the control limits are designed for the vibration signal from each individual tube, with no subgrouping required. A total of R control charts together monitor the vibration signals.

If the phase I performance of Hotelling T^2 control charts presents a small misdetection rate as well as a small false alarm rate, we recommend these T^2 control charts along with the historical $\bar{\boldsymbol{x}}_r$ and $\boldsymbol{S}_r$ for online monitoring. Otherwise, the proposed model needs to be revised in order to achieve a better performance. The model can be revised by (i) adjusting p value and hierarchical clustering in the tube quality classification step, (ii) modifying K value and F^* in the feature selection step, and (iii) adjusting the α value at the control chart development step.

It should be noted that the T^2 statistic is sensitive to the multivariate normality assumption. If the data are found to be not normally distributed, data preprocessing may be necessary. Using robust estimators of the centrality and dispersion parameters instead of the sample mean and sample covariance is also a popular approach to overcome data non-normality.

4 Case Study

In this section, the proposed methodology will be applied and validated through a total of four production batches with

Table 1 Description of production batches

Batch #	Number of tubes	Outer diameter (in.)	Wall-thickness (in.)	Usage in case study
1	16	3.938	0.360	Training
2	20	3.938	0.349	
3	15	4.500	0.338	
4	24	3.063	0.296	Validation

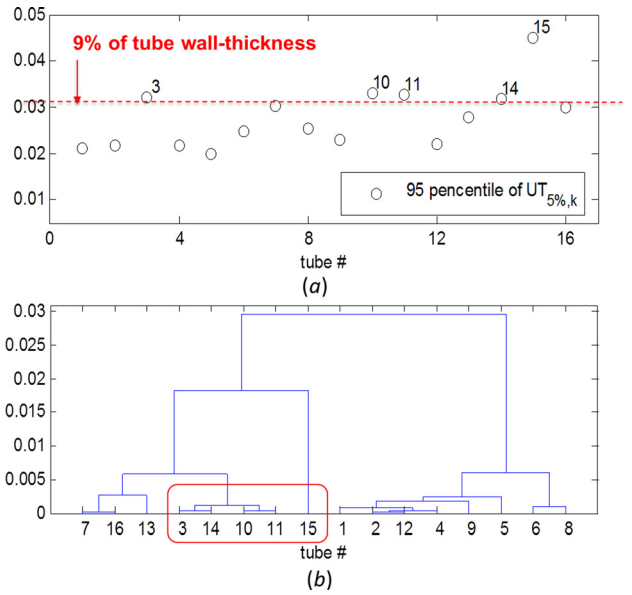

Fig. 14 Quality classification results for batch 1: (*a*) $U_{5\%,k}$ values and (*b*) dendrogram of hierarchical clustering

Table 2 Quality classification results

Batch #	High-quality group: Ω_0	Low-quality group: Ω_1
1	{1, 2, 4, 5, 6, 7, 8, 9, 12, 13, 16}	{3, 10, 11, 14, 15}
2	{2, 3, 4, 5, 6, 8, 9, 14, 16, 17, 18, 19, 20}	{1, 7, 10, 11, 12, 13, 15}
3	{1, 2, 3, 4, 6, 7, 8, 12, 14}	{5, 9, 10, 11, 13, 15}

Table 3 Indices of features with $S_0(f_i) = \emptyset$ and their corresponding $S_1(f_i)$ for batch 1

i	34	47	59	61	63	70	74	83	86	90	92
$S_1(f_i)$	15	10	10	10	10	10	10	3	3	14,15	11
i	95	99	103	111	123	143	147	148	149	157	
$S_1(f_i)$	10,15	10	10	15	10	10	10	10	10	19	

Table 4 Monitoring feature selection results for batch 1

	$\mathcal{F}$	V_1	V_0
Step 0	$\emptyset$	$\{3, 10, 11, 14, 15\}$	$\{1, 2, 4, 5, 6, 7, 8, 9, 12, 13, 16\}$
Step 1	$\{f_{90}\}$	$\{3, 10, 11\}$	Same as above
Step 2	$\{f_{90}, f_{47}\}$	$\{3, 11\}$	Same as above
Step 3	$\{f_{90}, f_{47}, f_{86}\}$	$\{11\}$	Same as above
Step 4	$\{f_{90}, f_{47}, f_{86}, f_{92}\}$	$\emptyset$	Same as above

Table 5 Summary of monitoring feature selection results

Batch #	F^*
1	$\{f_{47}, f_{86}, f_{90}, f_{92}\}$
2	$\{f_{90}, f_{92}, f_{97}, f_{117}\}$
3	$\{f_{47}, f_{52}\}$

tube-to-tube mapped data. The first three batches are treated as phase I data for model training and the last batch is used for model validation. Table 1 describes these four batches and their specifications. In Secs. 4.1–4.3, we present results on defining quality index, selecting monitoring features, and developing T^2 control charts, respectively. In Sec. 4.4, we further validate the proposed model on the fourth batch, which is treated as phase II data.

4.1 Defining Quality Index. Applying the clustering method proposed in Sec. 3.2, tubes in each batch are classified into high-quality tubes (Ω_0) and low-quality tubes (Ω_1). Take batch 1 for example, Fig. 14(*a*) plots the $U_{5\%,k}$ values for each tube k, and Fig. 14(*b*) shows the dendrogram from hierarchical clustering. Based on Fig. 14, low-quality tubes can be clearly distinguished from high-quality tubes, i.e., tube# 3, 10, 11, 14, and 15 are identified as low-quality tubes and the rest are high-quality tubes. This classification gives a cutoff value around 0.032, which is about 9% of the designed tube wall thickness. Table 2 gives a summary of tube quality classification results for all three training batches.

4.2 Monitoring Feature Selection. In Sec. 4.2, we discuss in detail on the selection of monitoring features for each training batch. As mentioned in Sec. 3.3, we first obtain $S_0(f_i) = \{k | y_{i,k} \geq H_i, k \in \Omega_0\}$ and $S_1(f_i) = \{k | y_{i,k} \geq H_i, k \in \Omega_1\}$ for each feature f_i, $i = 1, 2, \ldots, 160$ based on a threshold $H_i = \mu_i + K \cdot \sigma_i$ and $K = 3$, which corresponds to the widely used 3-sigma rule. The value of K can also be determined based on a prespecified α-risk (e.g., $\alpha = 0.27\%$). We then apply the greedy algorithm developed in Sec. 3.3 to determine $\mathcal{F}$. Since the objective function is $\left|\bigcup_{i:f_i \in \mathcal{F}} S_0(f_i)\right| + \lambda \sum_{i:f_i \in \mathcal{F}} w(f_i)$, we assign $\lambda = 0.05$, which puts false alarm as a highly undesirable situation.

Take batch 1 for example. Table 3 gives the indices of features that do not generate false alarms and the corresponding sets $S_1(f_i)$. Table 4 illustrates the steps in the greedy algorithm and the evolution of $\mathcal{F}$, V_1, and V_0 at each step.

With $\mathcal{F} = \{f_{90}, f_{47}, f_{86}, f_{92}\}$, the objective function is $\left|\bigcup_{i:f_i \in \mathcal{F}} S_0(f_i)\right| + \lambda \sum_{i:f_i \in \mathcal{F}} w(f_i) = 0 + 0.05 \times 4 = 0.2$. Since $H\left(\max_{i=1,2,\ldots,160} |S_i(f_i)|\right) = H(2) = 1.5$, the output of the objective function under $\mathcal{F}$, which is 0.2, is guaranteed to be no greater than 1.5 times of the optimum. The output of the objective function under the optimal solution should be greater than or equal to $0.2/1.5 = 0.13$. Since $0.13 < 1$, the optimal solution does not have false alarms, either. A closer look at Table 3 further tells us that it is infeasible to detect all low-quality tubes in $\Omega_1 = \{3, 10, 11, 14, 15\}$ using less than four features. Therefore, in this case, the greedy algorithm happens to find the optimal solution.

Table 5 summaries the feature selection results in all three training batches. For each batch, we obtain the monitoring feature set F^* which consists of frequency features that are sensitive to separating Ω_1 from Ω_0.

4.3 T^2 Control Chart Development for Selected Features. In this subsection, we provide details on the development of Hotelling T^2 control charts for each training batch. As mentioned in Sec. 3.4, we construct a T^2 control chart for each feature interval, $F_r (r = 1, 2, \ldots, R)$, while each F_r consists of a number of consecutive f_i's instead of individual features given in F^*.

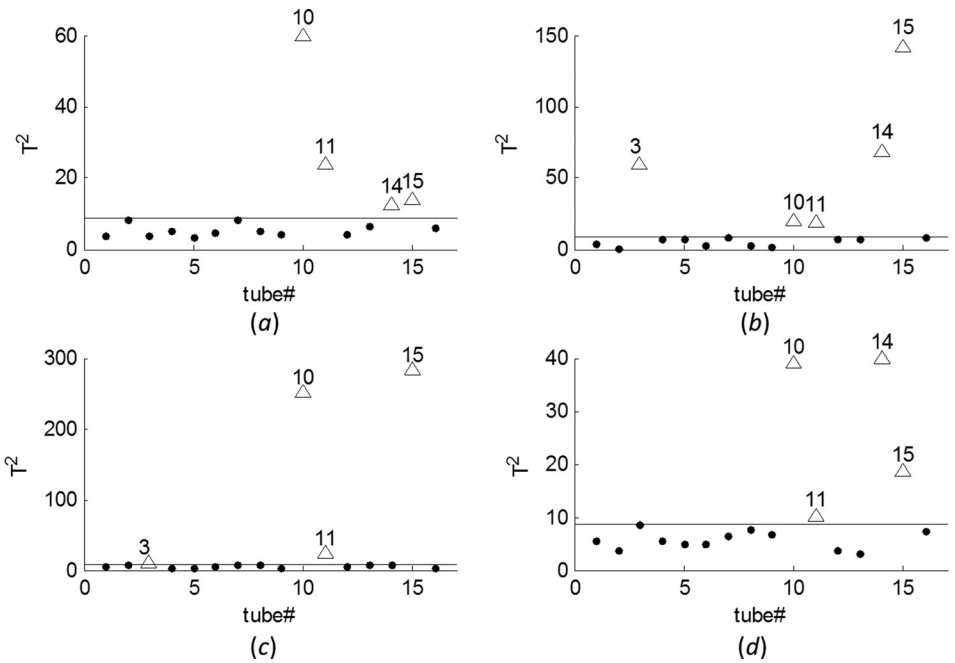

Fig. 15 T^2 control charts and monitoring results for batch 1: (*a*) monitoring features $F_1 = \{f_{47} \sim f_{52}\}$, (*b*) monitoring features $F_2 = \{f_{86} \sim f_{91}\}$, (*c*) monitoring features $F_3 = \{f_{92} \sim f_{97}\}$, and (*d*) monitoring features $F_4 = \{f_{115} \sim f_{120}\}$

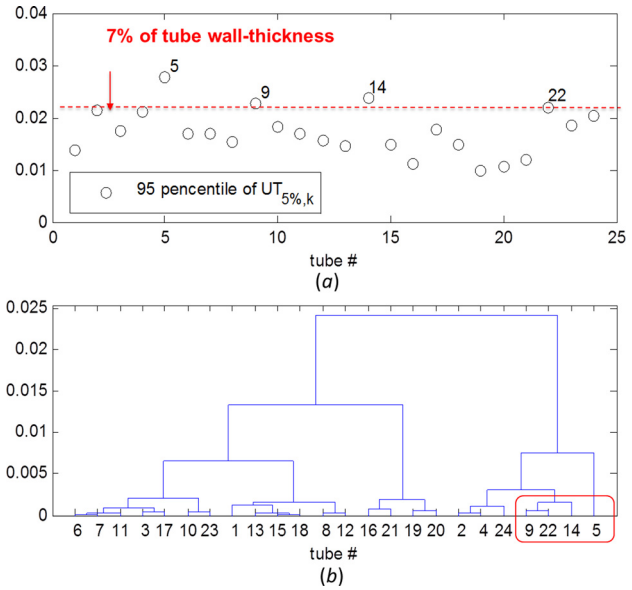

Fig. 16 Quality classification results for batch 4: (*a*) $U_{5\%,k}$ values and (*b*) dendrogram of hierarchical clustering

Based on the monitoring feature set F^* for each training batch given in Table 5, we determine $R = 4$ intervals of frequency features for Hotelling T^2 control charts: $F_1 = \{f_i : i = 47, 48, 49, 50, 51, 52\}$, $F_2 = \{f_i : i = 86, 87, 88, 89, 90, 91\}$, $F_3 = \{f_i : i = 92, 93, 94, 95, 96, 97\}$, and $F_4 = \{f_i : i = 115, 116, 117, 118, 119, 120\}$. Each feature interval contains six consecutive features covering approximately 2 Hz of vibrations frequencies.

Phase I control limits of the T^2 control charts are constructed for each batch separately using Eq. (5). In phase I, confidence level $\alpha = 0.01$ is chosen in order to achieve good detecting power with low false alarm rate. Take batch 1 for example. With $\alpha = 0.01$, phase I T^2 control charts are shown in Fig. 15, and Figs. 15(*a*)–15(*d*) give the T^2 control charts on the four feature intervals. In Fig. 15, the straight horizontal line indicates the upper control limit under $\alpha = 0.01$. A triangle represents an out-of-control T^2 statistic from a low-quality tube, while the dots represent in-control T^2 statistics. Therefore, triangles in Fig. 15 indicate true detection, while circles indicate false alarms. As can be seen from Fig. 15, all low-quality tubes are detected after combining the alarms from four feature intervals. Meanwhile, there is no false alarm generated in phase I. Therefore, the selected four feature intervals along with the corresponding phase II T^2 control limits are recommended for online monitoring. We further apply them on the validation dataset.

4.4 Validation for Online Monitoring Process. The fourth production batch is treated as phase II data in order to validate the developed monitoring technique. Batch 4 tubes are first classified into high-quality and low-quality groups, as shown in Fig. 16. Among a total of 24 tubes, tube#5, 9, 14, and 22 are identified as low-quality tubes since their wall-thickness variations are relatively high, and the rest tubes are defined as high-quality tubes. This classification gives a cutoff value around 0.022, which is about 7% of the tube wall thickness.

Four T^2 control charts are established for the four detecting feature intervals, and phase II limits are applied for online monitoring. As can be seem from Fig. 17, all four low-quality tubes (#5, 9, 14, and 22) can be successfully detected and only one false alarm (tube#20) is observed. The false alarm is indicated by the circle in Fig. 17(*c*), where the control chart monitors F_3: feature $f_{92} \sim f_{97}$. Hence, the proposed methodology is validated to be capable of detecting low-quality tubes with large wall-thickness variations and that the proposed technique can be applied to online monitoring of seamless tubes in hot piercing.

5 Discussion

We understand that the image-based sensing technique plays a vital role in this study. As the monitoring technique is developed based on information extracted from the images, the accuracy of sensory data needs to be guaranteed. Hence, operational characteristics of the sensing technique should be treated with caution. For example, the imaging system needs a working distance, from the tip of the imaging lens to the bar surface, greater than 100 mm [14] in order to reduce the chances of damage to the sensors and

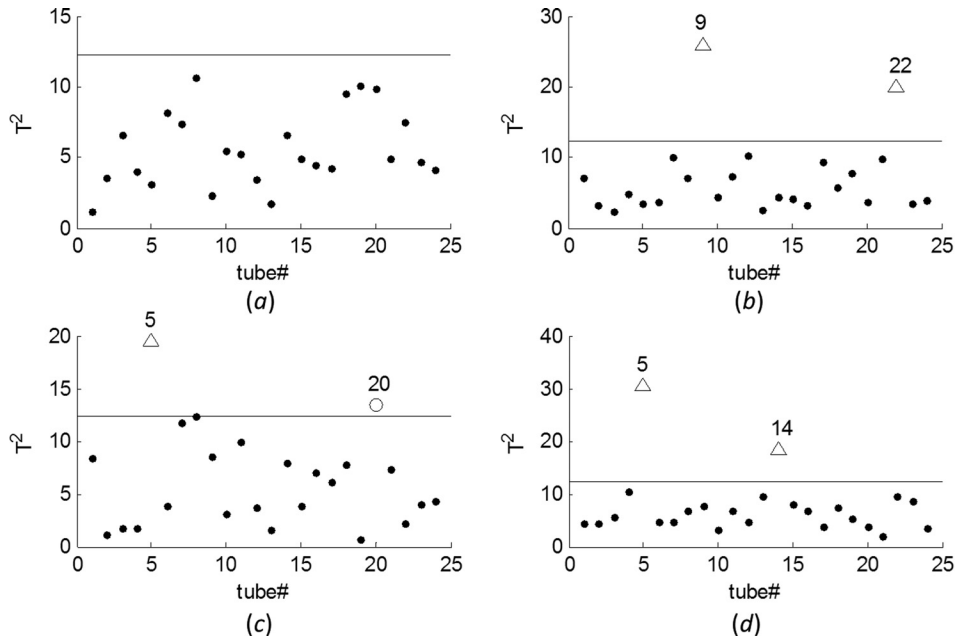

Fig. 17 T^2 control charts and monitoring results for batch 4: (*a*) monitoring features $F_1 = \{f_{47} \sim f_{52}\}$, (*b*) monitoring features $F_2 = \{f_{86} \sim f_{91}\}$, (*c*) monitoring features $F_3 = \{f_{92} \sim f_{97}\}$, and (*d*) monitoring features $F_4 = \{f_{115} \sim f_{120}\}$

allow a less stringent guiding requirement. The working distance should be consistent among the tubes in each production load so as to record comparable data. In order to process the vast amount of images in real-time, the sensing technique also needs to be equipped with a computing system and analysis algorithms. Future research will be conducted to further advance this process monitoring system with enhanced fault diagnosis capability using image data.

We mention in Sec. 2 that the UT data and vibration signals from normal production are normally load-to-load mapped rather than tube-to-tube mapped in industrial practice. Therefore, we propose to practitioners that a monitoring decision is made based on 3–4 consecutive alarms in a load given by the developed monitoring technique. Under this new decision-making strategy, not only the plant floor operator will have the flexibility to decide if the production of the current load should be paused for inspection, but also false alarms would be reduced and thus normal production would not be significantly affected.

Our recent studies have also discovered that the monitoring features and T^2 control limits are sensitive to the material grade of tubes. Moreover, significantly different dimensions of the tubes may also affect the monitoring features and T^2 control limits to a certain extent. In order to ensure the developed monitoring system is applicable to different products with different grades, the proposed monitoring technique can be further integrated with an adaptive learning approach to continuously learn/improve the knowledge database during production about the monitoring features selection and monitoring limits refinement. This adaptive learning approach aims to fully utilize the offline quality inspection data (from UT) based on the proposed principles to continuously improve on-line monitoring system performance. The refined monitoring approach will provide the capability of adaptive feature selection and control limits refinement based on continuously collected incoming training samples of defective tubes during production. This is one of next steps along this research.

6 Conclusion

This paper addresses the critical issue of online monitoring of eccentricity of seamless steel tubes in the cross-roll piercing mill. An online monitoring methodology is developed to detect abnormal vibration conditions using image sensing in the hot piercing process. Based on UT results of finished tubes, tubes in the training dataset are clustered into high-quality group and low-quality group according to the extent of their wall-thickness variations. Vibration signals collected from an image-based sensing technique are analyzed and process information is extracted. Frequency features that are sensitive to tube quality are then selected through the formulation of a set-covering problem and the solution given by a greedy algorithm. Based on the selected features, four Hotelling T^2 control charts are established using training data. The selected features and corresponding phase II control limits are then recommended for future online monitoring.

The developed monitoring technique enables early detection of eccentricity problems at the hot piercing stage. Instead of waiting for UT results of finished tubes, operators can receive timely alarms on abnormal conditions that contribute to eccentric tubes at the hot piercing stage. Such opportune alarms also facilitate timely adjustment and defect prevention. Generally, at least 3–5 batches of the production data are needed to train the monitoring technique for a new product/machine. Although the monitoring features and control limits may be different for tubes in different dimensions and materials, the developed monitoring technique is generic, which is applicable to the hot piercing process to obtain different monitoring features and/or control limits for various products. This paper also provides a general framework on effectively analyzing image-based sensing data and establishing the linkage between product quality information and process information.

Acknowledgment

This research was supported by the National Science Foundation under Award Nos. SBIR-0944614, SBIR-1058237, and DMI-1233108. The data in this study are provided by OG Technologies, Inc., and Michigan Seamless Tube & Pipe. The authors would like to thank Dr. Tzyy-Shuh Chang, Dr. Kamran Paynabar, Mr. Howard (Hsun-hau) Huang, and Mr. Tom Sleder for their help with process understanding and data collection.

References

[1] Oberg, E., and Jones, F. D., 1917, *Machinery's Encyclopedia: A Work of Reference Covering Practical Mathematics and Mechanics, Machine Design, Machine Construction and Operation, Electrical, Gas, Hydraulic, and Steam Power Machinery, Metallurgy, and Kindred Subjects in the Engineering Field, Industrial Press*, Machinery Publishing Co., New York\London.
[2] Mannesmannröhren-Werke, "Steel Tube and Pipe Manufacturing Processes," http://www.smrw.de/files/steel_tube_and_pipe.pdf
[3] Boljanovic, V., 2010, *Metal Shaping Processes: Casting and Molding, Particulate Processing, Deformation Processes, and Metal Removal*, Industrial Press, New York.
[4] DeGarmo, E. P., 2003, *Materials and Processes in Manufacturing*, Wiley, Hoboken, NJ.
[5] Zhao, Y. Q., and Mao, J. H., 2014, "Effects of Feed Angle on Mannesmann Piercing in Drill Steel Production," Adv. Mater. Res., **915**, pp. 915–916.
[6] Zhao, Y. Q., Yu, E. L., Hou, D. X., and Tang, X., 2013, "Effects of Plug Position on Mannesmann Piercing in Drill Steel Production," Appl. Mech. Mater., **385–386**, pp. 55–58.
[7] Liu, F., Qiu, Y. L., Song, Z. H., and Wang, S. W., 2013, "Numerical Simulation of the Piercing Process of Large-Sized Seamless Steel Tube," Appl. Mech. Mater., **319**, pp. 444–450.
[8] Birks, A. S., Robert, E., Green, J., and McIntire, P., 1991, *Ultrasonic Testing*, American Society for Nondestructive Testing, Columbus, OH.
[9] Hellier, C., 2003, "Chapter 7—Ultrasonic Testing," *Handbook of Nondestructive Evaluation*, McGraw-Hill, New York.
[10] Hirao, M. O. H., 2003, *EMATS for Science and Industry: Noncontacting Ultrasonic Measurements*, Kluwer Academic Publications, Boston, MA.
[11] Thompson, R. B., 1990, "Physical Principles of Measurements With EMAT Transducers," *Ultrasonic Measurement Methods*, Academic Press, New York.
[12] IMS Messsysteme GmbH, Heiligenhaus, Germany, "Measuring Systems in Tube Mills," http://www.imssystems-inc.com/pdf/IMS_Systems-TubeMeasurement.pdf
[13] Monchalin, J. P., Choquet, M., Padioleau, C., Néron, C., Lévesque, D., Blouin, A., Corbeil, C., Talbot, R., Bendada, A., Lamontagne, M., II, R. V. K., Jeskey, G. V., Dominik, E. D., Duly, L. J., Samblanet, K. J., Agger, S. E., Roush, K. J., and Mester, M. L., 2003, "Laser Ultrasonic System for On-Line Steel Tube Gauging," AIP Conf. Proc., **657**, pp. 264–272.
[14] Huang, H. H.-h., Gutchess, D., and Chang, T.-S., 2004, "Imaging-Based In-Line Surface Defect Inspection for Bar Rolling," AIST Iron and Steel Conference and Exposition, Nashville, TN, Sept. 15–17.
[15] Li, J., Shi, J., and Chang, T.-S., 2007, "On-Line Seam Detection in Rolling Processes Using Snake Projection and Discrete Wavelet Transform," ASME J. Manuf. Sci. Eng., **129**(5), pp. 926–933.
[16] Li, Q., Jin, J., and Chang, T.-S., 2010, "Detection and Diagnosis of Repetitive Surface Defects for Hot Rolling Processes," Trans. North Am. Manuf. Res. Inst. SME, **38**, pp. 615–622.
[17] Yang, Q., Li, Q., Jin, J., and Chang, T.-S., 2009, "Online Classification of Surface Defects in Hot Rolling Processes," Trans. North Am. Manuf. Res. Inst. SME, **37**, pp. 371–378.
[18] Li, Q., 2012, "Process Monitoring and Quality Control in Hot Rolling Processes Using Image Sensing Data," Ph.D. dissertation, University of Michigan, Ann Arbor, MI.
[19] Yang, Q., Jin, J., and Chang, T.-S., 2010, "Automatic Feature Extraction and Classification of Surface Defects in Continuous Casting," Trans. North Am. Manuf. Res. Inst. SME, **38**, pp. 563–570.
[20] Pan, E., Ye, L., Shi, J., and Chang, T.-S., 2009, "On-Line Bleeds Detection in Continuous Casting Processes Using Engineering-Driven Rule-Based Algorithm," ASME J. Manuf. Sci. Eng., **131**(6), p. 061008.
[21] Szekely, G. J., and Rizzo, M. L., 2005, "Hierarchical Clustering via Joint Between-Within Distances: Extending Ward's Minimum Variance Method," J. Classif., **22**(2), pp. 151–183.
[22] Brigham, E. O., 2002, *The Fast Fourier Transform*, Prentice-Hall, New York.
[23] Cormen, T. H., 2009, *Introduction to Algorithms*, MIT Press, Cambridge, MA.
[24] Li, J., and Jin, J., 2010, "Optimal Sensor Allocation by Integrating Causal Models and Set-Covering Algorithms," IIE Trans., **42**(8), pp. 564–576.
[25] Hotelling, H., 1931, "The Generalization of Student's Ratio," Ann. Math. Stat., **2**(3), pp. 360–378.